Electron diffraction methods for the analysis of silicon carbide surfaces and the controlled growth of polytype heterostructures

2004 J. Phys.: Condens. Matter 16 S1555

(http://iopscience.iop.org/0953-8984/16/17/008)

INSTITUTE OF PHYSICS PUBLISHING JOURNAL OF PHYSICS: CONDENSED MATTER

J. Phys.: Condens. Matter **16** (2004) S1555–S1578 PII: S0953-8984(04)67171-2

Electron diffraction methods for the analysis of silicon carbide surfaces and the controlled growth of polytype heterostructures

Aimo Winkelmann, Bernd Schröter[1] and Wolfgang Richter

Institut für Festkörperphysik, Friedrich-Schiller-Universität, Max-Wien-Platz 1, D-07743 Jena, Germany

E-mail: schroeter@pinet.uni-jena.de

Received 5 August 2003
Published 16 April 2004
Online at stacks.iop.org/JPhysCM/16/S1555
DOI: 10.1088/0953-8984/16/17/008

Abstract

The growth of different silicon carbide (SiC) polytypes on each other is possible by control of the surface structure and the appropriate thermodynamic parameters. Special ultrahigh vacuum conditions, like those used in solid source molecular beam epitaxy, allow the determination of the species on the surface and also the *in situ* characterization of the growing polytype by electron diffraction methods. The surface reconstruction which favours the growth of a certain polytype can be controlled by reflection high energy electron diffraction. For a non-destructive determination of the polytype of a grown thin SiC film, methods like x-ray photoelectron diffraction (XPD) and electron channelling can be used. The interaction length of electrons near 1 keV kinetic energy is in the range of 1 nm and therefore sensitive to the stacking sequence of the most common SiC polytypes 3C, 4H, 6H with *c*-axis dimensions between 0.75 and 1.5 nm. To prepare polytype heterostructures like 4H/3C/4H or 6H/3C/6H, untwinned 3C SiC films without double-positioning boundaries have to be grown. On-axis α-SiC substrates with uniform surface stacking termination are a prerequisite for this. Such surfaces can be prepared using high temperature hydrogen etching, sublimation etching or step-flow growth. These equally terminated crystals with threefold surface symmetry are particularly suitable for detailed studies of the atomic-geometric structure and their changes during growth or after certain treatments. Results of surface-sensitive characterization methods like scanning tunnelling microscopy, XPD and low energy electron diffraction are presented.

(Some figures in this article are in colour only in the electronic version)

[1] Author to whom any correspondence should be addressed.

1. Introduction

1.1. Polytype heterostructures

The concept of semiconductor heterostructures consisting of a single material in different crystal modifications is an exciting idea which may lead to novel applications in electronic devices [1, 2]. Up to now, heterostructures are usually grown from different materials such as GaAs and AlAs. The problems that occur when trying to match the interfaces of both materials may be circumvented by the use of a single material. Silicon carbide (SiC) has been shown to be one of the most promising materials in this field because it occurs in several modifications (polytypes) which can be stacked on each other with practically no lattice mismatch (figure 1).

Among the potential applications, there are two very interesting devices for SiC heteropolytype structures: the high electron mobility transistor (HEMT) [3] for high frequency, high power electronics and the quantum cascade laser (QCL) [4] for optical emitters in the near-infrared.

Despite the very amazing results of GaN/AlGaN HEMTs, these devices suffer from the lattice mismatch of AlN and GaN. The Al content of the AlGaN gate is limited to about 30% to prevent an unfavourably high interface roughness between the gate and the GaN channel material. The interface roughness leads to electron scattering and, as a consequence, to a limitation on the electron drift velocity. A hypothetical SiC polytype HEMT consists of a hexagonal SiC gate electrode with a large bandgap on top of the cubic SiC channel material, both materials grown on the Si face of a hexagonal SiC(0001) polytype. Due to the very small in-plane lattice mismatch of the different SiC polytypes the interface can be expected to be smooth and therefore no extra electron scattering takes place. Together with the high thermal conductivity of SiC and the intrinsic pyroelectric field, high performance SiC polytype HEMTs can be expected.

The group IV semiconductors suffer from their indirect band structure concerning their potential application for active optoelectronic devices. As SiC polytype heterostructures show the main band discontinuity in the conduction band, heterostructures of the type 6H/3C/6H or 4H/3C/4H are expected to form a quantum well in the conduction band. At a quantum well thickness of only a few nanometres, the well contains more than one electronic state and, consequently, intersubband transitions are possible. Therefore, the successful QCL concept with III–V semiconductors may be used to construct such an optical emitter using a stack of SiC heteropolytype structures. This can pave the way for integration of high frequency HEMT devices with unipolar light emitters in the near-infrared region on the material base of group IV semiconductors.

For the successful production of polytype heterostructures, the crystal structure of the growing films has to be engineered on thickness scales of a few nanometres. Apart from controlling surface structure and the thermodynamic conditions which lead to the formation of a specified polytype, a non-destructive thin-film polytype determination during or after growth of only a few atomic layers is a great challenge. Conventional techniques like x-ray diffraction (XRD), Raman scattering and photoluminescence (PL) can provide non-destructive polytype information for bulk samples and thick films but are less surface-sensitive. Due to the short inelastic mean free paths of electrons with low and medium energies, electron diffraction techniques are sensitive to only a few atomic layers. This is why we have concentrated on electron diffraction techniques.

In this paper, we will review the progress that has been made in the field of thin film SiC polytype growth by molecular beam epitaxy and we will show how electron diffraction methods can be applied for non-destructive analysis of the grown films. In the main part we will review the methods of x-ray photoelectron diffraction (XPD) and electron channelling (EC) and will discuss some applications and results on thin-film polytype determination.

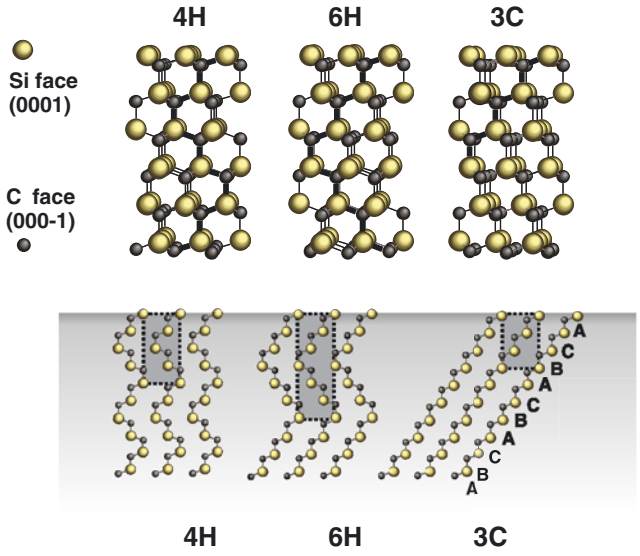

Figure 1. SiC polytypes 4H, 6H, 3C and their $(11\bar{2}0)$ plane.

Additionally, we will present recent results on the potentiality of reflected high energy electron diffraction (RHEED) for *in situ* polytype identification as well as results obtained on unit-cell terminated α-SiC surfaces.

1.2. Growth and formation of silicon carbide polytypes

Over the last 40 years much experimental and theoretical knowledge on the growth and formation of SiC polytypes has been achieved.

The occurrence of different polytypes dependent on the temperature has been studied in sublimation experiments under near-equilibrium conditions [5]. Factors affecting the crystal polytype are the temperature and the pressure in the growth chamber, the polarity of the seed crystal, the presence of certain impurities and the Si/C ratio. Under more Si-rich (C-rich) conditions the formation of the cubic (hexagonal) polytype should be preferred [6]. Nucleation far from equilibrium conditions has been generally assumed to give the cubic polytype [7–9]. This is supported by nucleation theory. 3C SiC has the lowest surface energy and a small cubic nucleus consisting of mainly surface atoms will be stable at high supersaturation. All these effects can also influence the epitaxial layer growth. Additionally, the variety of surface superstructures changing the surface energy play a role in the epitaxial growth process, especially at temperatures below 1500 K [10–14].

High-quality SiC has usually been grown by chemical vapour deposition (CVD). A step-flow growth mode on vicinal (off-oriented) SiC(0001) reproduces the substrate polytype and results in homoepitaxial layers which have reached a quality suitable for device application. By nucleation on the terraces of well-oriented SiC(0001) substrates, the cubic 3C SiC polytype is always grown by CVD. By sublimation epitaxy at high temperatures, different polytypes have been obtained by varying the temperature and Si/C ratio [15, 16]. High-quality SiC layers can be grown by high temperature CVD at high growth rates and under Si-rich conditions [17]. Gas-source MBE has been used to grow cubic and hexagonal SiC layers [18–20].

Few growth experiments have been done by solid-source molecular beam epitaxy (SSMBE) using electron guns for the evaporation of silicon and carbon [21–24].

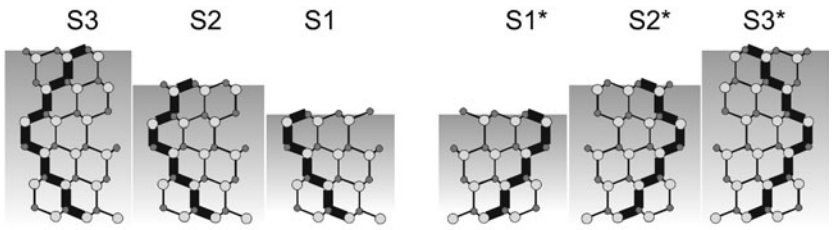

Figure 2. Stacking terminations of 6H SiC.

Contrary to CVD or gas-source MBE, there are simpler conditions at the surface as only a few different species are involved. SSMBE allows an easy control of the growth process and the surface stoichiometry, which is a prerequisite for the formation of different polytypes via nucleation. The surface stoichiometric conditions are related to surface superstructures which can be observed by RHEED during MBE. Models of the most common superstructures on hexagonal SiC surfaces have been proved by low-energy electron diffraction (LEED), scanning tunnelling microscopy (STM) and photoelectron spectroscopy [25–27].

Recently, Fissel *et al* [28–30] succeeded in the realization of SiC polytype heterostructures like 4H/3C/4H by careful control of the surface superstructure and the thermodynamic conditions during MBE growth. The regions of homogeneous formation of the polytype on 3C SiC were found to be in the range of some microns [29] and are likely to be limited by surface and bulk-related defects.

A prerequisite for the growth of cubic SiC without twin boundaries is a uniform stacking termination of the hexagonal on-axis SiC substrate surfaces (figure 2). Correspondingly, a careful surface preparation of the substrates characterized by a low defect density is important.

2. The controlled growth of SiC polytype heterostructures by MBE

2.1. Review of the previous experimental results

The growth of certain polytype heterostructures by controlling the surface superstructure and stoichiometry under well-defined thermodynamic conditions has been described by Fissel *et al* [29–32]. SSMBE under ultrahigh vacuum (UHV) conditions allows the *in situ* characterization of the surface superstructure and growth by RHEED. We will briefly review the results of these investigations.

Before growth, the on-axis substrate surfaces were prepared by wet chemical treatment and plasma etching [33]. No ordered step structure has been observed after this *ex situ* treatment. *In situ* the samples were prepared by sublimation etching at high temperatures of 1600 K in a Si flux, resulting in surface steps of 2–6 Si–C bilayers (BLs) in height in the case of 6H SiC(0001) and of 1–4 BL in the case of 4H SiC(0001). Subsequently, a SiC buffer layer has been grown at the same temperature and Si flux but with additional carbon flux [31]. At these conditions the growth rate was low enough to prevent nucleation even on the nominal on-axis substrates, leading to a step morphology with unit-cell step heights predominating.

Growing 3C SiC on a hexagonal SiC polytype, the occurrence of domains with different stacking orientations and their incoherent twin (double-position) boundaries in between has to be prevented. Fissel *et al* [29–32] have shown that the growth of 3C SiC on on-axis substrates can be significantly improved by an alternating supply of Si and C, especially at a rather high temperature >1500 K. Single-domain 3C SiC was obtained on α-SiC(0001) in lateral

dimensions of some millimetres. Small regions of cubic SiC in twin positions were found to be only associated with surface imperfections like scratches or bulk defects. Although the lattice parameters of cubic and hexagonal SiC polytypes differ slightly, no difference has been found in the in-plane lattice constant between the 3C layer and the hexagonal SiC substrates, whereas the lattice constants in the growth direction are different. This means that the cubic layers grow pseudomorphically on hexagonal α-SiC(0001) [34].

Further growing SiC at even higher temperature near 1600 K under C-rich conditions on the 3C SiC layer at the same growth rate results in the formation of 4H on top of the cubic layer grown on 4H SiC(0001) or of 6H when the 3C layer was grown on 6H, respectively. The C-rich conditions can be checked by the occurrence of the $(\sqrt{3} \times \sqrt{3})$R30° superstructure spots in the RHEED pattern. That superstructure is formed by a Si adlayer of $1/3$ monolayer on top of the SiC surface [35].

The regions of homogeneous formation of the hexagonal polytypes on 3C SiC had lateral dimensions of some microns, likely to be limited by bulk and surface-related defects. The preferential formation of the α-SiC polytypes at low supersaturation and C-rich conditions agrees very well with estimations performed within the framework of nucleation theory [32]. However, the formation of either only a 4H/3C/4H or a 6H/3C/6H heterostructure indicates an influence of the strain within the layers on the growing polytype.

2.2. What has to be done?

Summarizing previous experimental results, the controlled growth of SiC heteropolytypic structures consisting of hexagonal and cubic polytypes has been performed by SSMBE. The quality of the polytype heterostructures is limited by defect-induced inhomogeneities and very critical experimental conditions which require a careful *in situ* characterization of the surface superstructure as well as of the polytype or stacking sequence of the upper SiC layer. Techniques to determine the polytype of a very thin SiC layer nondestructively have to be used *in situ*. We will describe several electron diffraction methods sensitive to the polytype structure in the main part of this paper.

Obviously, bulk and surface-related defects limit the homogeneity of the heterostructures. Substrate surface preparation is crucial for high-quality polytype growth. The *in situ* sublimation etching in a Si flux at 1600 K before MBE growth is rather expensive and, apparently, not sufficient to yield low-defect substrate surfaces.

High-temperature hydrogen or HCl/H_2 etching has been known to result in a step morphology with atomically flat terraces and a characteristic stacking termination or step bunching [36–39]. On the other hand, surface roughening after hydrogen etching has been reported, indicating the strong dependence on etching conditions and crystal quality. There are a few studies on the effects of on-axis 6H SiC substrate etching on the quality of epitaxial SiC layers [40, 41]. Hydrogen etching was effective in removing 3C nucleation sites and reducing double-positioning boundaries. The preferential occurrence of half or full unit-cell high steps on etched surfaces has been reported [36–39, 42]. It was suggested that step bunching is a surface equilibrium process with different surface energies of each additional SiC BL [7, 8, 43–45]. The formation of steps half a unit cell high can be explained by the different growth velocities of S1, S2 and S3 steps for the case of 6H SiC (figure 2). Due to the different number of dangling bonds, the two half-unit cell stacking sequences ABC and ACB advance at different speeds v_{ABC} and v_{ACB} and thus may form a unit cell size step [46].

We have used high temperature hydrogen etching to prepare unit-cell terminated 6H and 4H SiC{0001} substrate surfaces on both Si or C faces (figure 3). The unit-cell termination is a prerequisite for the growth of single-domain 3C SiC in polytype heterostructures. The 6H

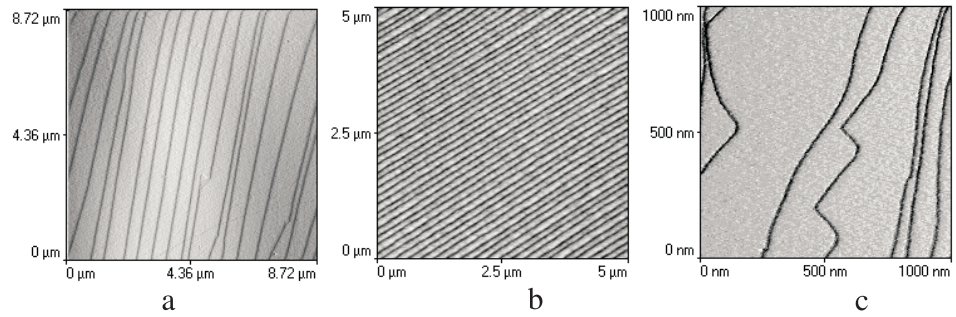

Figure 3. Atomic force micrographs of (a) a Si face of 4H SiC, (b) a Si face of 6H SiC and (c) a C face of 6H SiC after hydrogen etching, showing unit-cell step heights and wide atomically flat terraces.

or 4H SiC substrate surfaces show a threefold pattern in surface-sensitive electron diffraction experiments like LEED, XPD or EC. We will present first the results of such investigations on both polar faces of α-SiC surfaces showing threefold surface symmetry because of homogeneous unit-cell termination.

3. Non-destructive determination of the thin-film polytype and surface stacking termination by electron diffraction

The structure of SiC surfaces directly influences the processes of oxidation, thin film growth and polytype change [47]. This is one reason why clean and oxidized SiC surfaces have been investigated with a number of different surface analysis methods, including qualitative analyses of surface stoichiometry and symmetry by electron spectroscopy methods and LEED [25, 27, 48–63] as well as STM [64–68].

To quantitatively analyse the atomic structure of ultrathin SiC films, electron diffraction methods are well suited because of the short information depth attainable with low and medium energy electrons. To be sensitive to at least the unit-cell size of the polytypes 3C, 4H and 6H, the sphere of action of the electron diffraction effects has to extend to a depth of about 2 nm. This corresponds to electron energies in the region of 1 keV or more. One can use elastically scattered electrons from an external source or electrons which are excited inside the thin film to be analysed. For instance, LEED and diffraction of photoelectrons excited by x-rays (XPD) as well as the analysis of backscattered electrons (EC patterns and electron backscatter diffraction (EBSD)) can be used. Especially in MBE growth experiments, RHEED is applied. Polytype specific effects can be observed with all of the above methods. Simulations of the observable diffraction effects have been proven to be of great value for the unambiguous identification of polytype stacking sequences near a thin film surface. In the following, we will give a short review of the experimental methods applicable to ultrathin SiC films, explain briefly the theoretical concepts relevant to simulations and give examples of applications of these methods.

3.1. Experimental methods

3.1.1. X-ray photoelectron diffraction. A photoelectron which was emitted by an atom excited by x-rays can be scattered by the neighbouring crystal atoms (figure 4). This causes variations of the photoelectron current, depending on the emission angle and provides a possibility to analyse the crystal structure near the emitting atom. Electrons with energies

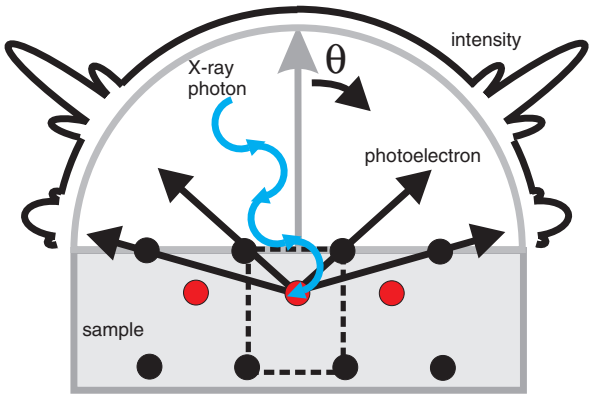

Figure 4. Principle of XPD.

above 500 eV are scattered mainly in the forward direction. Because of this, emitter-to-scatterer directions show up as maxima in the angular photoemission intensity distribution, which makes possible a relatively easy interpretation of the resulting angular photoelectron distributions.

The measured two-dimensional intensity patterns can be displayed in a stereographic projection. In figure 5, a Si 2p intensity distribution of 3C SiC(111) is shown with the corresponding crystal directions and traces of the reflecting planes. Also shown is the connection between the crystal structure and our experimental coordinate system with azimuth angle ϕ and polar angle θ. The relationship between close packed directions and forward scattering maxima is clearly distinguishable.

SiC has been recently investigated using XPD by a number of groups, addressing the problems of surface reconstructions [69, 70] and substrate emission [71–73]. With synchrotron radiation, the chemical shift of the surface atoms could be used for photoelectron diffraction [74]. Most of the publications deal with 6H or 3C SiC. The growth of 3C on 6H was analysed by XPD [75, 76]. A systematic study of polytype specific effects was carried out by our group [77–79].

Our experimental set-up consists of a x-ray source with an Al/Mg twin anode and a concentric hemispherical analyser. The sample can be computer-controlled rotated in polar and azimuthal directions to acquire a number of angle resolved spectra. These can be automatically analysed for intensity in the corresponding photoelectron peak and drawn either as a one-dimensional polar plot or a two-dimensional stereographic projection using custom-made software. The experimental x-ray photoelectron spectra of Si 2p and C 1s were acquired using Mg Kα (1254 eV) and Al Kα (1487 eV) radiation. The binding energies of about 100 eV for Si 2p and 284 eV for C 1s result in photoelectron kinetic energies of 1387/1154 eV (Si 2p) and 1203/970 eV (C 1s) for Al/Mg Kα excitation, respectively.

3.1.2. Electron channelling and electron backscatter diffraction. Dynamical interaction of a diffracted electron beam with a crystalline sample leads to variations in the backscattered current with sample orientation. If these variations are measured synchronously with the rocking of a parallel beam on the sample, an electron channelling pattern (ECP) results. Angle resolved variations in the backscattered electron current with a stationary electron beam lead to EBSD. *In situ* observation is possible using a conventional UHV electron gun. Backscattered electrons can be collected by a channeltron or semiconductor detector in the case of ECP and by phosphor screens or microchannel plates in the case of EBSD. Data collection and processing is done with a PC.

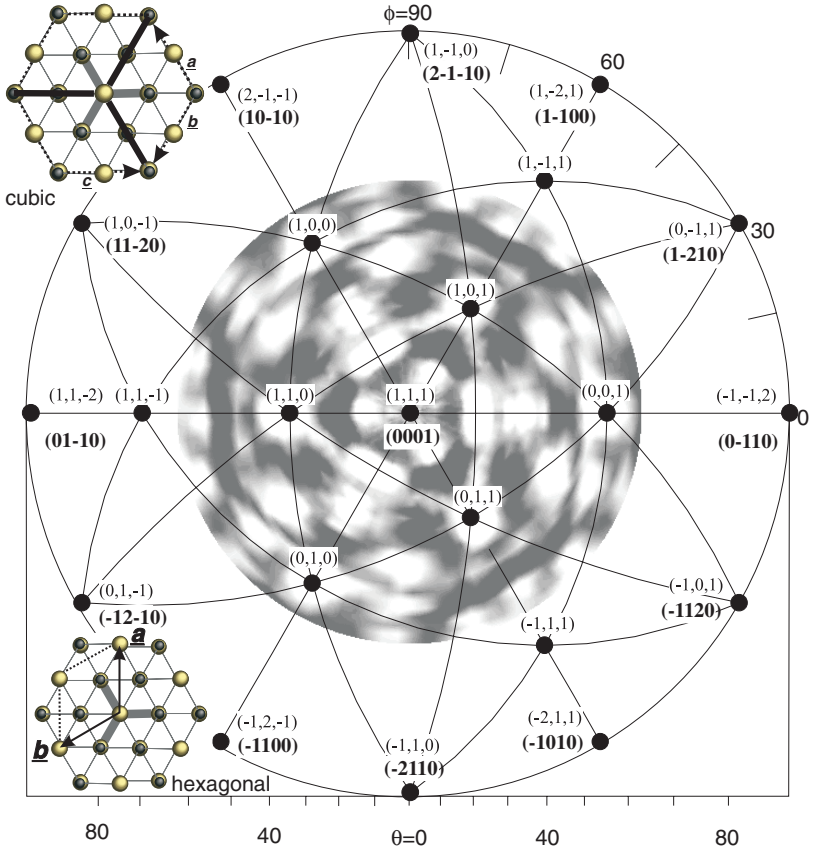

Figure 5. Stereographic projection of Si 2p photoelectron intensities of 3C SiC(111) and the relationship between crystal structure and experimental coordinate system.

ECP and EBSD provide various kinds of information [80, 81]. The patterns show the symmetry elements of the crystal structure and can be used for the identification of symmetry axes and mirror planes [82]. Orientation determination of crystals and crystallites is possible because of the fixed relative positions of the channelling patterns and the sample. The quality of the crystal is reflected by the sharpness of the patterns. That is why ECP and EBSD have been used for analysis of the quality of epitaxially grown films [83–87] and for the quantification of ion implantation damage [88]. Crystal defects can be imaged by EC because they create a contrast [89].

The principle of our experimental set-up is shown in figure 6. The measurements were carried out in an UHV chamber equipped with a STAIB EK-12-M electron gun capable of delivering an electron beam with energies of up to 12 keV. This gun is also used for Auger electron spectroscopy and low resolution scanning electron microscopy. The beam energies can be continuously varied. The backscattered electrons were collected either using a channeltron or a photomultiplier type of detector which gave equivalent results. The sample was positively biased with 50 V to suppress secondary electrons. Image acquisition and electron beam scanning was computer controlled. The beam is adjusted to be parallel while it is scanned over the surface. Thus its angle relative to the surface changes. This leads to variations of the backscattered electron current which are displayed on the computer. The variations in

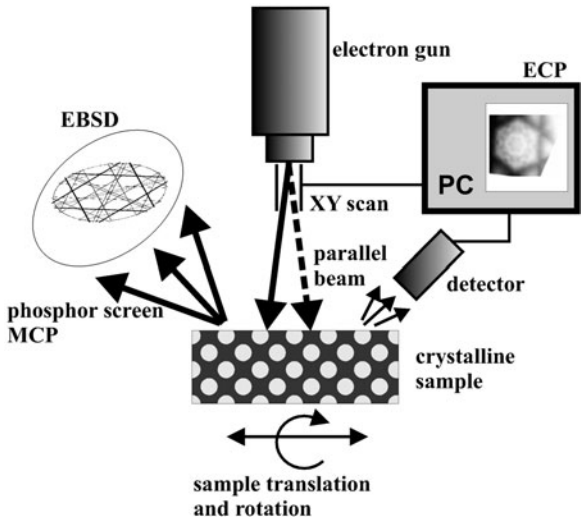

Figure 6. Principle of ECPs and EBSD.

backscattered current amount to less than 5%, which makes necessary a careful adjustment of signal amplification and image processing by the computer software.

ECP and EBSD have been used for the analysis of SiC samples. For instance, a very fast polytype identification is possible by taking ECPs near the (0001) direction [90, 91]. Damage on a crystalline 4H SiC surface can also be evaluated by ECP [92]. Layer spacing measurements in EBSD have been shown to be of use for the analysis of SiC polytypes [82].

3.1.3. Low energy electron diffraction. Elastic scattering of low energy electrons (LEED) is a standard surface-analytical technique. In combination with dynamical simulations, LEED measurements are a powerful tool for the determination of the structure of adsorbates and surface reconstructions.

Quantitative LEED was successful in the determination of the structure of SiC surface reconstructions and led to models of the atomic arrangement of a number of surface structures. It was demonstrated in a number of publications how the power of LEED can be used on SiC surfaces. They found models for the (3×3) [26, 93, 94] and $(\sqrt{3} \times \sqrt{3})$R30° reconstructions [13] on SiC(0001). C faces were analysed in [95, 96], the step structure of SiC surfaces with different stacking terminations was determined [97–99] and the problems of surface oxidation and passivation were investigated [100–103]. The central role of the surface structure for a controlled growth of SiC was pointed out [13, 14, 100, 104].

At energies above 0.5 keV, LEED will be sensitive to more than just the top layer of the surface. Thus, information on stacking sequences can be gained. However, reliable measurements of I–V data at these energies are very difficult because of the increasing influence of inelastic scattering. Electrons which experienced phonon losses are the source of the so-called Kikuchi patterns. The energy loss of the Kikuchi electrons is less than 1 eV (quasielastic scattering) and they can be thought of as originating from point sources located at the atomic nuclei. This leads to a close analogy between these Kikuchi patterns and photoelectron diffraction.

3.1.4. Reflection high energy electron diffraction. Elastic reflection of high energy electrons at grazing incidence (RHEED) is a standard tool for the *in situ* characterization of thin film growth by MBE. The grazing incidence of the electron beam leads to a surface

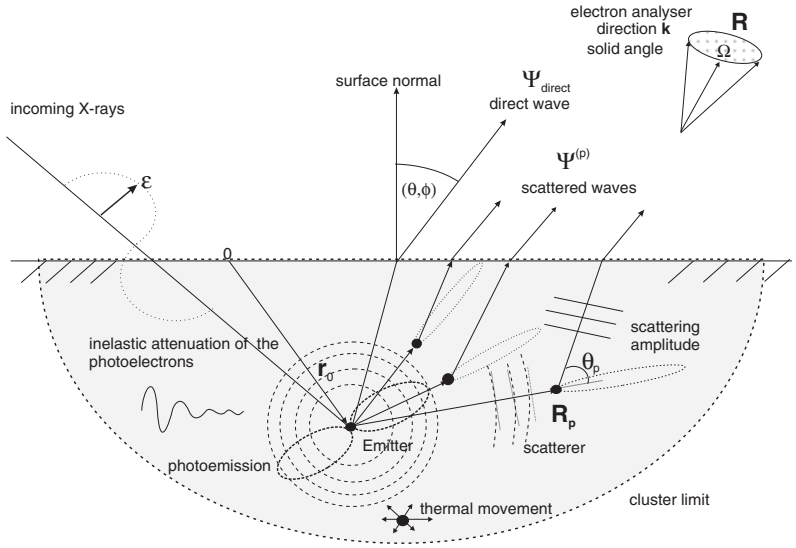

Figure 7. SSC model of XPD.

sensitivity comparable to LEED. Together with the absence of energy filtering in RHEED, this makes polytype differentiation by elastic RHEED patterns rather difficult, because inelastic electrons may contribute a dominating part to the diffraction pattern. However, kinematic simulations have shown that polarity and polytype determination could be possible under ideal conditions [105].

As in LEED, inelastic scattering in RHEED can lead to the formation of Kikuchi patterns. Because of the specific geometry of the RHEED set-up, the Kikuchi lines can be caused from one-, two- or three-dimensional periodicities [106, 107] at the surface. The Kikuchi lines of the polytype-specific three-dimensional lattice planes can be used for the determination of the polytype [108, 109].

3.2. Theory and simulation

3.2.1. XPD. We have used a single scattering cluster (SSC) model to simulate the effects of XPD on ultrathin SiC films (figure 7). The SSC model used in our calculations is described by Fadley in [110]. In this model, the outgoing photoelectrons are scattered only once by a neighbouring atom. The intensity which is scattered by such an atom is described by a scattering factor calculated from the phase shifts of the angular momentum components of an incoming plane wave. In addition, the effects of inelastic scattering, thermal attenuation of the scattered amplitudes and the limited angular resolution of the analyser have to be taken into account. The SSC model was incorporated into a computer program which allows simulations of single scattering XPD patterns from arbitrary bulk and surface structures.

The phase shifts needed for the calculations have been derived from a muffin-tin potential using the Barbieri–Van Hove phase shift package [111]. Values of the inelastic attenuation length have been obtained using the Tanuma–Powell–Penn (TPP) formula [112]. A fitting procedure for the attenuation length showed that it had to be reduced by a factor of 1.5 compared to the TPP formula [113]. The Debye temperature of SiC was taken to be around 1300 K [114]. For comparison with experimental data, the angular resolution of the analyser

(2°) was simulated by summing up the intensities from a number of different directions that fall into the analyser solid angle.

Calculations using the plane wave SSC model tend to overestimate the intensity along atomic chains. This can be corrected in part by the use of spherical wave scattering [115, 116]. Our calculations for the emission of the Si 2p and C 1s core levels in SiC excited by Al/Mg Kα radiation have shown that the experimental curves are equally well described by an empirical reduction of the plane wave scattering amplitudes [113].

The size of the hemispherical cluster of atoms considered has been increased until no further changes in the diffraction pattern took place. This leads to a cluster radius around 25 Å, which is equivalent to more than 3000 atoms. This large cluster size is necessary because of the long inelastic mean free path (>20 Å) of the Si 2p and C 1s electrons emitted. Large numbers of atoms have been shown to be necessary to simulate all the fine structure of substrate core level emission [113] but user-friendly programs for full scale multiple scattering calculations are currently limited to several hundred atoms [117]. This is why we used the single scattering approach.

In order to minimize the influence of the instrumental response function, we used polar χ curves for the comparison between experiment and theory, $\chi = (I - I_0)/I_0$, with I_0 being a smooth background fitted to the experimental polar scan intensities I by means of a polynomial spline fitting method [117, 118]. In the case of full hemispherical patterns, I_0 should not depend on the azimuth and can be estimated by taking the average value of all intensities at the particular polar angle and smoothing the background obtained in the polar direction. In this way, all diffraction effects in the background are eliminated [119]. For comparison of the calculated and measured curves, we used R-factor routines supplied in a program of the MSCD package [117]. In most of our calculations, we considered the surface as bulk-terminated and disregarded any effects due to surface reconstructions. It has been shown that this can safely be done due to the relatively high kinetic energy of the photoelectrons [120, 121].

3.2.2. Dynamical theory of electron channelling patterns. The variations of the backscattered electron current which form the ECP are due to dynamical diffraction effects of the incoming electron beam with wavevector $\mathbf{k}_0$. We have used a Bloch wave approach to describe the diffraction of the incoming electrons. The use of this method is described in several reviews (e.g. [122, 123]). In the following, we give a short summary of the basic theory we applied.

The wavefunction inside the crystal is described as a superposition of Bloch waves with wavevectors $\mathbf{k}^{(j)}$:

$$\Psi(\mathbf{r}) = \sum_j c_j \exp(2\pi \mathrm{i}\mathbf{k}^{(j)} \cdot \mathbf{r}) \sum_g C_g^{(j)} \exp(2\pi \mathrm{i}\mathbf{g} \cdot \mathbf{r}) \tag{1}$$

with three-dimensional reciprocal lattice vectors $\mathbf{g}$. Substituting these Bloch waves into the Schrödinger equation leads to the standard dispersion relation

$$[\mathbf{K}^2 - (\mathbf{k}^{(j)} + \mathbf{g})^2]C_g^{(j)} + \sum_h U_{g-h}^{\mathrm{c}} C_h^{(j)} = 0. \tag{2}$$

The crystal potential is described by complex electron structure factors $U_g^{\mathrm{c}} = 2m|e|V_g/h^2$, with V_g being a Fourier coefficient of the total crystal potential in volts and the relativistic electron mass m. $\mathbf{K}$ is the electron wavevector inside the crystal, $k_0^2 = 1/\lambda^2 = K^2 - U_0^{\mathrm{c}}$. One then writes $\mathbf{k}^{(j)}$ as $\mathbf{k}^{(j)} = \mathbf{K} + \gamma^{(j)}\mathbf{n}$, where $\mathbf{n}$ is a unit vector normal to the surface and neglects elastic backscattering to transform (2) into an eigenvalue problem which gives the eigenvalues $\gamma^{(j)}$ and eigenvectors with elements $C_g^{(j)}$. The boundary conditions at the surface determine the coefficients c_j in (1). After this, the wavefunction (1) is known and can be used to calculate the electron current density inside the crystal.

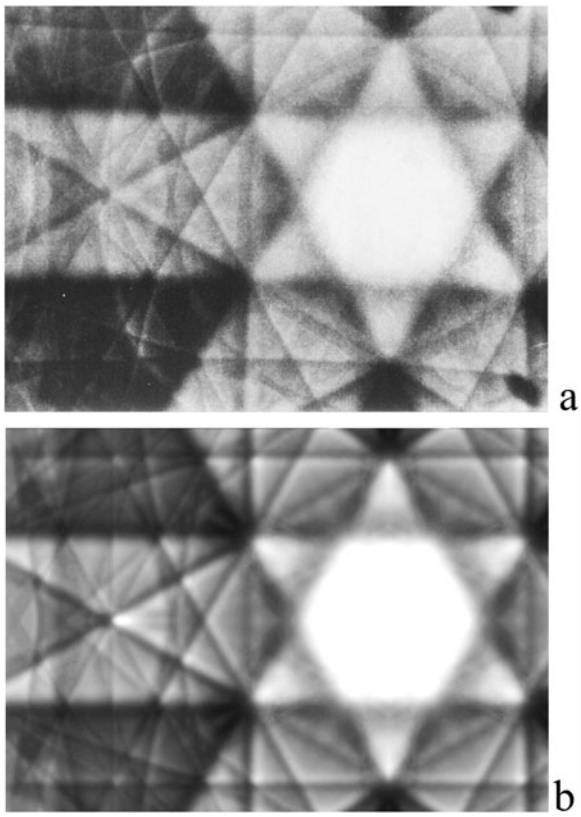

Figure 8. ECP of 6H SiC (0001) at 15 kV. (a) Experiment, (b) dynamical simulation using 247 reflecting planes.

Attenuation of the incoming beam is described by an imaginary component of the crystal potential which was calculated by use of the ATOM subroutine from [124]. The Fourier coefficients of the real part of the crystal potential were taken from [125]. The Debye–Waller factors we took from a parametrization from [126].

To describe the inelastic backscattering of the diffracted electrons, one can imagine that increased backscattering will take place if the electrons have a higher probability to be near the atomic cores. Increased phonon creation will then lead to a higher amount of backscattering [127]. So, in principle one has to take the wavefunction (1) and compute the probability of the diffracted electrons to be near the atomic cores and weight the result by the square of the atomic number of the scatterer and its Debye–Waller factor to account for the strength of the scattering and thermal effects [128]. Diffraction effects of the outgoing electrons were not considered due to the large enough ($>10°$) acceptance angle of the detector.

For calculation of the Bloch waves, we have used a program published by Zuo *et al* [123, 129] which is usually applied to convergent beam electron diffraction (CBED). We modified this code to include the backscattering effects according to the above outlined approach. In this way we could simulate the ECPs (figure 8).

Many-beam effects in ECPs have been studied before by Marthinsen [130] and Rossouw [128]. Further simulations were done by Dudarev [131] using an inhomogeneous transport equation approach for the inelastically scattered electrons.

3.2.3. LEED and RHEED. Because of the importance of multiple scattering effects at energies used in LEED, a dynamical theory has to be used to explain the dependence of the spot intensity on the electron energy (I–V curve). We applied the SATLEED package [111] for the simulations which were compared to the experimental I–V curves.

At higher energies near 1 keV, LEED patterns are dominated by inelastic effects. The formation of Kikuchi patterns caused by phonon scattered electrons is observed. These electrons can be thought to originate from point sources at the atomic cores, which leads to a close analogy with photoelectron diffraction. This is why LEED Kikuchi patterns can also be successfully modelled with a cluster approach.

In our SSC model, the inelastically scattered electrons were thought to originate isotropically from Si and C atoms scaled with the square of the atomic number to take into account the different phonon creation cross sections of Si and C. The remaining elastically scattered electrons cause a spot diffraction pattern and were also modelled using the cluster approach. The incoming plane wave was scattered at each atom at $\mathbf{R}_j$ according to the complex scattering amplitude $f_j(\Delta\mathbf{k})$ and the scattered waves were summed up coherently to give the elastically scattered intensity in an angular direction specified by the change in wavevector $\Delta\mathbf{k}$. To account for inelastic attenuation with the distance L_j travelled in the material, an exponential damping term $\exp(-L_j/2\lambda)$ was applied with the inelastic mean free path λ. The Debye–Waller factor $\exp(-M_j)$ accounts for the thermal damping of the scattering amplitude. This SSC model can be summed up in a modified kinematical formula for the scattered amplitude:

$$A_{\Delta\mathbf{k}} = \sum_j f_j(\Delta\mathbf{k}) \exp(-M_j) \exp(\mathrm{i}\Delta\mathbf{k}\mathbf{R}_j) \exp(-L_j/2\lambda). \tag{3}$$

The elastic and inelastic intensities were calculated for the complete angular range visible in the LEED pattern and showed the characteristic spot pattern superimposed with the Kikuchi bands. It cannot be assumed that the simulated spot pattern reflects all the observed relative intensities and possible absences of spots because dynamical effects are completely neglected. The spot pattern is merely used qualitatively to compare the positions of the inelastic features relative to it.

The observed Kikichu lines in the RHEED set-up were also compared to kinematical simulations. These were carried out using the program 'Electron Diffraction' [132].

3.3. Applications

3.3.1. Polytype and polarity determination by XPD. The arrangement of atoms surrounding an emitter of photoelectrons leads to intensity variations of the angular photoelectron intensity. There are specific changes of the local structure around silicon and carbon emitters in different SiC polytypes. These variations can be used for polytype determination by XPD.

In figure 9 we show specific scattering directions which enable the differentiation between 6H SiC and 4H SiC. Because the specified scattering atoms are at relatively long distances away from the emitters, the observed effects are small in comparison to the dominating forward scattering directions to the nearest silicon atoms. This emphasizes a careful alignment of the samples and sufficient long measuring times to optimize the signal-to-noise ratio. Experimental photoelectron intensity plots and the corresponding simulations for the case illustrated in figure 9 can be found in [79].

Two-dimensional photoelectron diffraction patterns of Al Kα excited Si 2p photoelectrons of 6H, 4H and 3C SiC are shown in figure 10. The corresponding SSC simulations reproduce the characteristic differences of these patterns, depending on polytype and polarity. Multiple scattering effects can have a notable influence along densely packed directions [79].

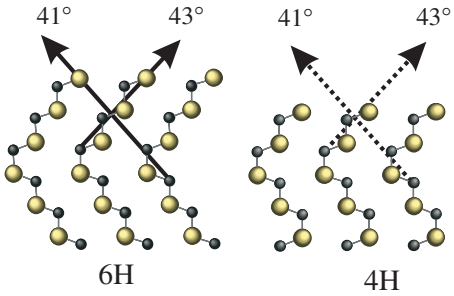

Figure 9. Characteristic scattering directions around a C 1s emitter in the $(11\bar{2}0)$ plane of 6H SiC (full arrows). These scattering directions are missing in 4H SiC (broken arrows).

Based on film growth experiments and emitter resolved simulations, one can estimate the information depth of XPD in SiC. We have found that, at photoelectron energies of about 1–2 keV, this depth amounts to a maximum of about 8–10 double layers or approximately 20 Å [79].

3.3.2. Polytype determination by electron channelling patterns. The possibility to use ECPs for polytype determination of thin surface layers of SiC was described in [90]. There it was shown that, in order to identify the polytypes, it is sufficient to change the angle of incidence of the electron beam by ± 40 mrad relative to the surface normal coinciding with the [0001] symmetry axis of a crystal. ECPs at 9.25 keV for the basic SiC polytypes 3C, 4H, 6H, 8H, 15R, 21R, 27R and 33R were presented.

For the analysis of ultrathin SiC films, we have used energies in the range from 2 to 8 keV. Characteristic patterns can be observed at a number of energies which enables the use of this method in a fingerprint mode [91]. The observed patterns could be explained by the use of many-beam dynamical simulations using a Bloch wave model (figure 11) [133, 134].

3.3.3. Kikuchi lines in RHEED for polytype determination. For the controlled MBE growth of SiC polytype films it would be desirable to distinguish the grown polytype directly on the RHEED screen. The symmetry of the RHEED diffraction pattern is based on the symmetry of the two-dimensional surface layers. Because the different polytypes are built up from the same two-dimensional layers, polytype information cannot be gained from the symmetry of the RHEED diffraction pattern. However, differences in the stacking sequence should manifest themselves in intensity variations along the rods of the reciprocal space which are seen as streaks on the RHEED screen. These variations are caused by the influence of the periodicity normal to the surface layer and thus could supply polytype information. As in LEED, the intensity variations are also strongly influenced by dynamical effects due to the atomic structure of the surface layer [106]. The effects due to polytype, surface reconstructions, partial surface disorder and inelastically scattered electrons are superimposed in the final diffraction pattern. Together with the experimental set-up of RHEED, which usually does not include energy filtering as in LEED, this poses a difficulty for the experimental confirmation of polytypic differences in the elastic diffraction pattern which have been found in kinematical simulations [105].

Because of the strong influence of inelastically scattered electrons in RHEED, diffraction effects of these electrons can also be used for polytype determination. The resulting Kikuchi lines have the advantage that one can rely on line positions and positions of line crossings and not on the measurement of elastic intensities over an unknown inelastic background.

Kikuchi line measurements for polytype determination in RHEED have been first proposed by Zhukova *et al* [108, 109], who also gave explicit formulae for their experimentally

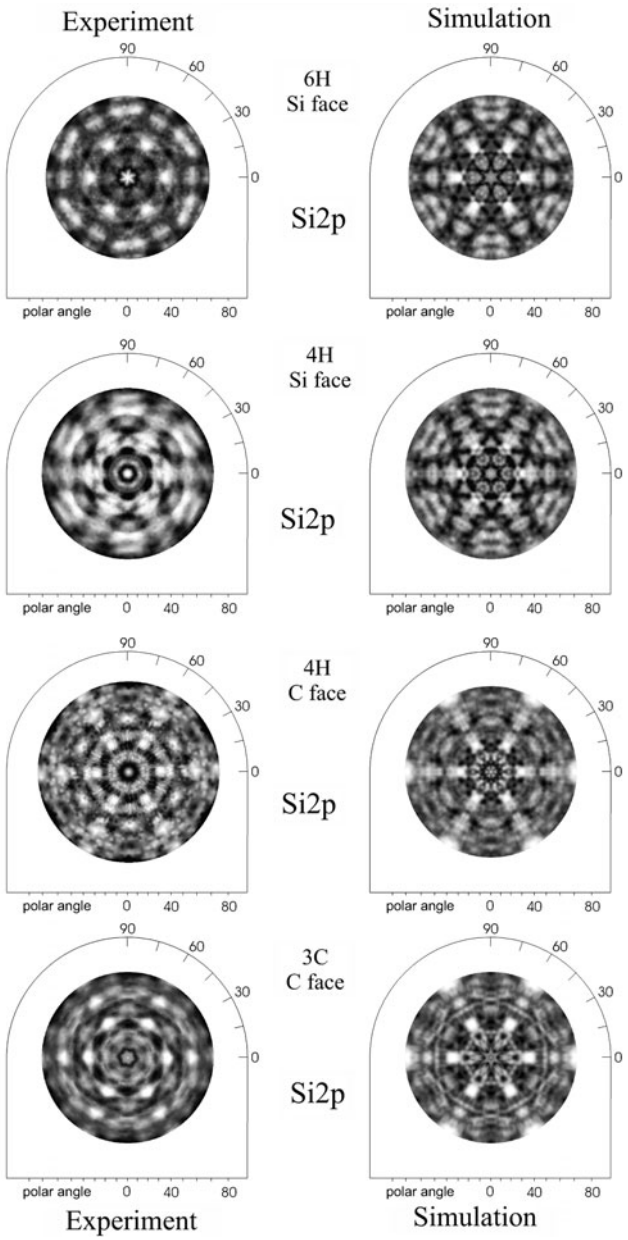

Figure 10. Measured Si 2p photoelectron diffraction patterns and comparison with SSC simulations.

determined Kikuchi line positions. To be consistent with the notation in [108, 109], a hexagonal coordinate system with three indexes (hkl) is used in this section.

Only reflections (h, k, l) with $h - k \neq 3n$ are sensitive to a change of the stacking sequence [108]. For polytype determination in RHEED, the lines which belong to the first group or reflexes with $h^2 + hk + k^2 = 1$ are especially useful: $(h, k) = (0, 1), (1, 0), (1, -1), (0, -1), (-1, 0), (-1, 1)$.

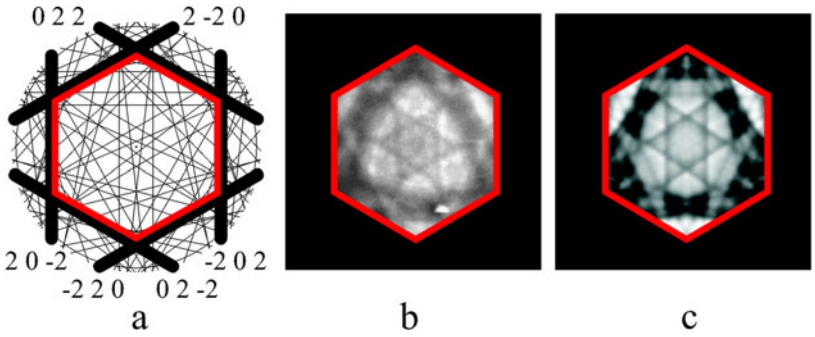

Figure 11. ECP of 3C SiC(111) at 4000 eV. (a) Kinematical pattern, (b) experiment, (c) dynamical simulation [133].

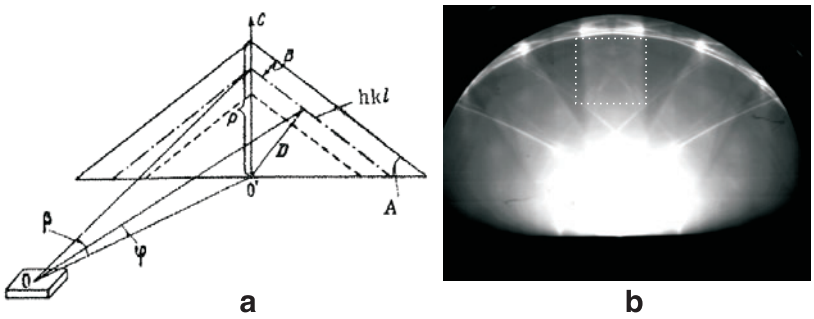

Figure 12. (a) Coordinate system for measuring Kikuchi lines on the RHEED screen [108]. (b) RHEED pattern of a 6H SiC(0001) surface with the area marked which is used for polytype determination, azimuth [2 1 0].

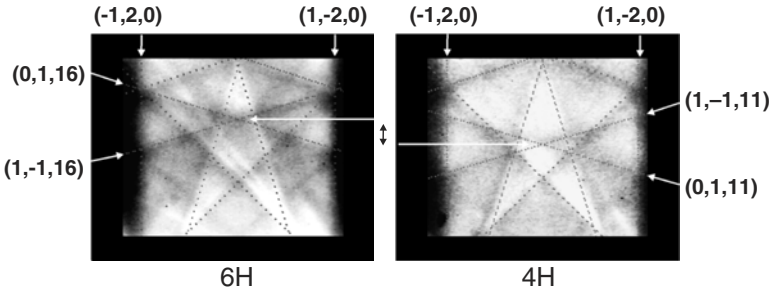

Figure 13. Differentiation between 4H and 6H SiC by RHEED Kikuchi lines at 35 kV.

In [108] RHEED patterns of 6H and 15R at 75 kV were analysed. We have examined the most common polytypes 3C, 4H and 6H. In figure 12(b) we show a RHEED Kikuchi pattern of 6H SiC(0001) which was taken in our SiC-MBE chamber at 35 kV. Because of the limited dynamics of the video camera, the central area is heavily overexposed. The broken rectangle marks the area with lines which can be used for polytype determination. For 4H and 6H, this area is shown enlarged in figure 13.

The lines shown correspond to kinematic simulations and were calculated with the program 'Electron Diffraction' [132]. One can clearly distinguish the change of positions of the lines $(1, \bar{1}, 11)$ and $(0, 1, 11)$ at 4H as well as $(1, \bar{1}, 16)$ and $(0, 1, 16)$ at 6H in comparison to the lines which are at the same positions for both polytypes.

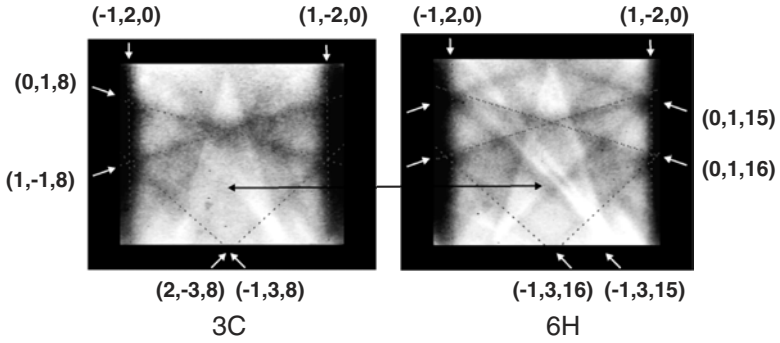

Figure 14. Differentiation between 6H and 3C by RHEED Kikuchi lines at 35 kV (hexagonal coordinate system with $c = 7.55$ Å for 3C and $c = 15.17$ Å for 6H).

The reflexes mentioned in [108] are also useful for the differentiation between 3C and 6H. One only has to keep in mind that a doubling of the layer constant in real space leads to a reciprocal space layer constant which is half as large. There are twice as many reflections for 6H as for 3C which show up as additional lines. In figure 14 we show RHEED Kikuchi pictures of a 3C thin film and a 6H SiC substrate. Clearly one can see additional lines at 6H. The 3C pattern is indexed in a hexagonal coordinate system with a c axis of 7.55 Å to see the systematic changes in the Miller indices. At 6H, the l index of a (hkl) line shared with 3C is twice as large as at 3C because of the longer c axis. However, 6H lines with an odd l, have no counterpart at 3C and are the characteristic sign of 6H.

In summary, we have shown how polytype determination of 4H, 6H and 3C is possible with RHEED Kikuchi patterns.

3.3.4. Surface stacking termination. The surface stacking termination of SiC samples was investigated by Starke *et al* using LEED. It was shown that it is possible to determine the area ratios of domains with different stacking termination by quantitative LEED analyses [99] with error margins of the mixing ratios of about ±20% [95]. Polytypes with statistically mixed terminations are difficult to distinguish while samples with preferential terminations show larger differences [97]. The LEED simulations showed that detection of stacking faults between the third and fourth layers (S3 and S4 termination) poses the limit of this method because of the short inelastic mean free paths of low energy electrons [97].

3.3.5. Unit-cell terminated SiC surfaces. An effective method of surface preparation of SiC is etching in hot hydrogen gas at temperatures of about 1700–1800 K. Ideally, this leads to surfaces which are terminated by flat terraces with step heights of half or full unit-cell sizes. Surfaces prepared this way are well suited for MBE growth of polytype heterostructures. The terraces have widths of up to 1 μm, depending on the off-axis angle of the sample. In this section we show the results of investigations on C-face 6H SiC$(000\bar{1})$.

STM. The 6H SiC$(000\bar{1})$ sample was investigated by STM. A surface morphology was found which consisted of steps with an equal step size of one unit cell (figure 15). This is consistent with a surface which is almost uniformly terminated by the same stacking termination. Because the STM does not give information about deeper layers, XPD and LEED have been used to determine the stacking sequence near the surface. This can be used to give a model of the stepped surface.

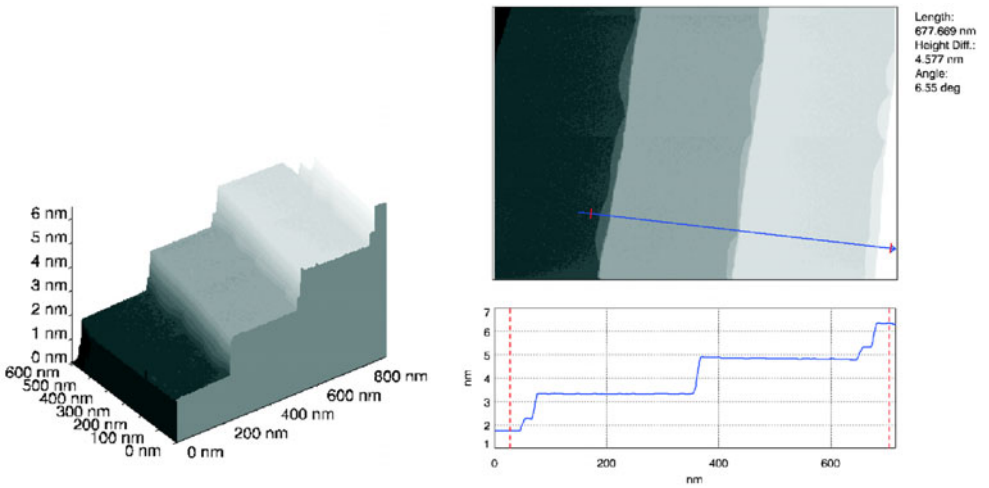

Figure 15. STM picture of the hydrogen-etched 6H SiC(000$\bar{1}$) sample.

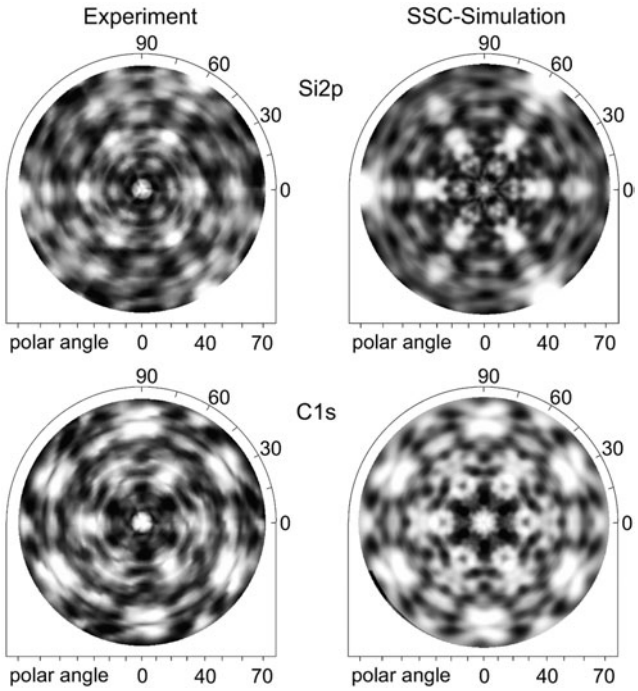

Figure 16. XPD patterns of 6H SiC(000$\bar{1}$) Al Kα excitation of Si 2p and C 1s, experiment and SSC simulation.

XPD. A uniformly terminated surface should show a threefold symmetry using surface-sensitive electron diffraction methods like XPD and LEED. In the case of XPD, the photoelectron angular distributions of Al Kα-excited Si 2p and C 1s electrons were analysed. The corresponding intensity maps are shown in figure 16. The pattern shows a threefold symmetry which supports the assumption of a uniformly terminated surface. A statistical termination would lead to a sixfold pattern.

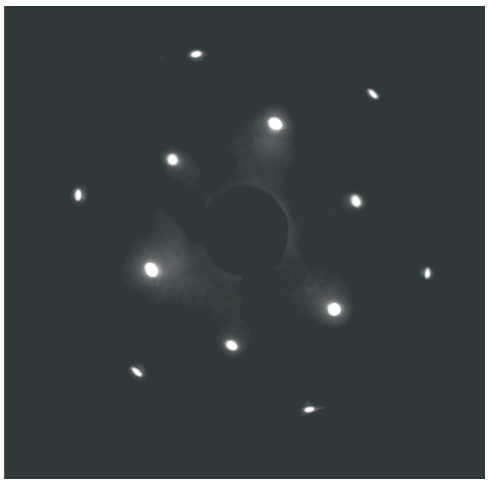

Figure 17. Threefold LEED pattern of a 6H SiC(000$\bar{1}$) surface, 124 eV.

Table 1. *R*-factor comparison for different terminations of the hydrogen-etched 6H SiC(000$\bar{1}$) sample.

Termination	R_{Pendry}
S1	0.64
S1*	0.44
S2	0.37
S2*	0.72
S3	**0.17**
S3*	0.52
S4	0.27
S4*	0.55

On the right side of figure 16, the SSC simulations for a S3-terminated surface are shown. These reproduce the experimental patterns very well. The S3 termination was supported in an *R*-factor analysis of the XPD polar plots.

LEED. In figure 17 a LEED pattern is shown, which was observed on the 6H SiC sample. There is a clear threefold symmetry which has to come from the uniform termination of the sample. Effects due to surface reconstructions or adsorbates can be ruled out from XPS measurements. Such effects should show the same symmetry as the underlying substrate as long as there is no adsorbate which arranges itself independently of the substrate. So, in any case a uniform stacking termination of the substrate would be the basis for a threefold symmetry of the diffraction pattern.

LEED *I*–*V* measurements were carried out and compared with dynamical simulations. In the simulations a clean surface with no adsorbates was considered with atoms at the positions of the bulk crystal. Eight terminations were considered which are listed in table 1 together with the corresponding Pendry *R* factors. The best factor of 0.17 was found for the S3 termination. The much worse *R* factor of the S3* termination shows the strong threefold symmetry of the pattern. This means that there is only a small part of the domains present which are rotated by 60°. If both domains were present in equal amounts, this would lead to a sixfold symmetry of the pattern. In figure 18 we show measured *I*–*V* data and simulated curves of the S3 termination.

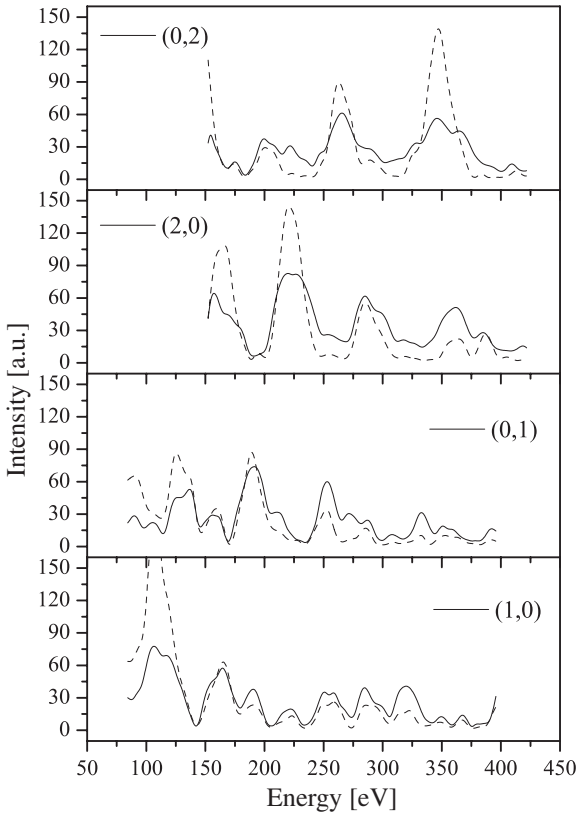

Figure 18. LEED I–V measurements (full curves) of the 6H SiC(000$\bar{1}$) sample and dynamical simulations (broken curves) for S3 termination, $R_{\text{Pendry}} = 0.17$.

In the next step, we tried to consider a mixture of different terminations. The largest change in the R factor was found for a mixture of 90% S3 and 10% S3* with a Pendry R factor of 0.13. An error margin was determined from the variance of the Pendry R factor at the minimum with $\text{var}(R_{\min}) = \sqrt{8V_{0i}/\Delta E}$, with ΔE being the measured energy range [135]. From the error interval, the amount of S3 termination can be estimated as 80–100%.

For the uppermost layers, a slight compression was found which was less than 0.05 Å, which is within the experimental error. A strong compression of 40% (0.63–0.38 Å) in the first layer of the C face was predicted theoretically [136]. The absence of compression could be caused by saturation of the dangling bonds. Because LEED is not very sensitive to small amounts of hydrogen or oxygen at the surface, the presence of these atoms cannot be ruled out. This was also found in a different investigation of 6H SiC(0001) [95], where surface models with adatoms could not be differentiated from the clean bulk surface.

The LEED I–V data of the 6H SiC(000$\bar{1}$) sample was taken in the energy range from 200 to 400 eV. At higher energies, inelastic effects begin to dominate the diffraction pattern and Kikuchi bands are observed. The Kikuchi pattern at 1000 eV, which is given in figure 19, also shows the threefold symmetry. We applied the SSC model to calculate the elastic spot pattern and the Kikuchi bands. For a cluster of 15 Å radius and S3 termination, the superimposed inelastic and elastic patterns in figure 19 reproduce the experimentally observed structures quite well. The relative positions of the elastic and Kikuchi patterns match up and the threefold symmetry of both patterns is also reproduced.

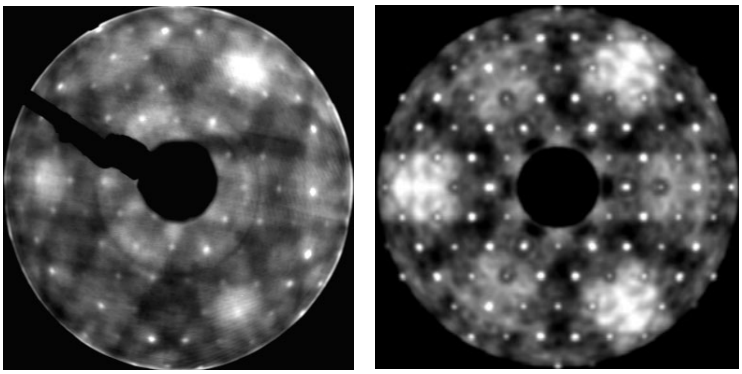

EXPERIMENT SSC SIMULATION

Figure 19. Kikuchi patterns of the uniformly S3-terminated 6H SiC sample at 1000 eV and comparison to SSC simulation.

We have shown how the combination of various analysis methods can lead to a picture of the step structure on hydrogen-etched SiC samples. The investigations by STM, XPD and LEED convincingly support the assumption of uniform S3 termination of the 6H SiC$(000\bar{1})$ sample analysed. Similar results have been found on the Si face of 6H SiC after hydrogen etching.

4. Summary

The current progress in the growth of polytype heterostructures by SSMBE has been reviewed. The growth of different SiC polytypes on each other is possible by control of the appropriate thermodynamic parameters and analysis of the growing crystal structure. UHV conditions allow the determination of the species on the surface and also the *in situ* characterization of the growing polytype by electron diffraction methods.

For a non-destructive determination of the polytype of a very thin SiC film, methods like XPD and ECP can be used. The interaction length of electrons near 1 keV kinetic energy is in the range of 1 nm and is therefore sensitive to the stacking sequence of the most common SiC polytypes 3C, 4H and 6H with c-axis dimensions between 0.75 and 1.5 nm. Additionally, Kikuchi lines observed in RHEED patterns can be used for polytype identification.

To prepare polytype heterostructures like 4H/3C/4H or 6H/3C/6H, untwinned 3C SiC films without double-positioning boundaries have to be grown. α-SiC substrates with uniform surface stacking termination are a prerequisite for this. Such surfaces can be prepared using high temperature hydrogen etching, sublimation etching or step-flow growth.

We have used high temperature hydrogen etching to prepare unit-cell terminated 6H and 4H SiC$\{0001\}$ substrate surfaces on both Si or C faces. These crystals show threefold surface symmetry and are particularly suitable for detailed studies of the atomic-geometric structure and their changes during the growth or certain treatments. Results of surface-sensitive characterization methods like STM, XPD and LEED were presented.

The power of electron diffraction methods with low to medium energy electrons lies in its ability to sample a number of surface layers which makes these methods very suitable for non-destructive *in situ* UHV measurements of ultrathin crystalline films.

Acknowledgment

We thank A Fissel for providing samples of MBE-grown SiC layers.

References

[1] Bechstedt F and Käckel P 1995 *Phys. Rev. Lett.* **75** 2180
[2] Murayama M and Nakayama T 1994 *Phys. Rev.* B **49** 4710
[3] Weisbuch C and Vinter B 1991 *Quantum Semiconductor Structures* (San Diego, CA: Academic)
[4] Capasso F 1999 *Semiconductor Quantum Electronics* ed A Miller, M Ebrahimzadeh and D M Finlayson (Bristol: Institute of Physics Publishing) p 391
[5] Knippenberg W F 1963 *Philips Res. Rep.* **18** 161
[6] Omuri M, Takei H and Fukuda T 1989 *Japan. J. Appl. Phys.* **28** 1217
[7] Heine V, Cheng C and Needs R J 1991 *J. Am. Ceram. Soc.* **74** 2630
[8] Limpijumnong S and Lambrecht W R L 1998 *Phys. Rev.* B **57** 12017
[9] Tairov Y M and Tsevtkov V F 1981 *J. Cryst. Growth* **52** 146
[10] Fissel A, Kaiser U, Ducke E, Schröter B and Richter W 1995 *J. Cryst. Growth* **154** 72
[11] Fissel A, Kaiser U, Pfennighaus K, Schröter B and Richter W 1996 *Appl. Phys. Lett.* **68** 1204
[12] Furthmüller J, Käckell P, Bechstedt F, Fissel A, Pfennighaus K, Schröter B and Richter W 1998 *J. Electron. Mater.* **27** 848
[13] Starke U, Schardt J, Bernhardt J, Franke M and Heinz K 1999 *Phys. Rev. Lett.* **82** 2107
[14] Grossner U, Fissel A, Furthmüller J, Richter W and Bechstedt F 2001 *Mater. Sci. Forum* **353–356** 211
[15] Vodakov Y A, Mokhov E N, Ramm M G and Roenkov A D 1979 *Krist. Technik* **14** 729
[16] Mokhov E N, Shulpina I L, Tregunova A S and Vodakov Y A 1981 *Cryst. Res. Technol.* **16** 879
[17] Kordina O *et al* 1996 *Appl. Phys. Lett.* **69** 1456
[18] Fuyuki T, Yoshinobu T and Matsunami H 1993 *Thin Solid Films* **225** 225
[19] Yoshinobu T, Mitsui H, Izumikawa I, Fuyuki T and Matsunami H 1992 *Appl. Phys. Lett.* **60** 824
[20] Kern R S, Jährendahl K, Tanaka S and Davis R F 1997 *Phys. Status Solidi* b **202** 379
[21] Kaneda S, Sakamoto Y, Nishi C, Kanaya M and Hannai S I 1981 *J. Cryst. Growth* **81** 536
[22] Zenkentes K, Callec R, Tsagaraki K, Sagnes B, Arnaud G, Pascual J and Camassel J 1995 *Mater. Sci. Eng.* B **29** 138
[23] Petzoldt J, Stauden T, Cimalla V, Ecke G, Romanus H and Eichhorn G 1998 *Mater. Sci. Forum* **264–268** 251
[24] Kitabatake M 1998 *Mater. Sci. Forum* **264–268** 327
[25] Starke U 1997 *Phys. Status Solidi* b **202** 475
[26] Starke U *et al* 1998 *Phys. Rev. Lett.* **80** 758
[27] Johansson L I, Owman F and Martensson P 1996 *Phys. Rev.* B **53** 13793
[28] Fissel A, Schröter B, Kaiser U and Richter W 2000 *Appl. Phys. Lett.* **77** 2418
[29] Fissel A 2001 *J. Cryst. Growth* **227/228** 805
[30] Fissel A, Kaiser U, Schröter B, Richter W and Bechstedt F 2001 *Appl. Surf. Sci.* **184** 37
[31] Fissel A, Kaiser U, Schröter B, Kräußlich J and Richter W 2000 *Thin Solid Films* **380** 89
[32] Fissel A 2000 *Thin Solid Films* **212** 438
[33] Ducke E, Kriegel R, Fissel A, Kaier U, Schröter B, Müller P and Richter W 1996 *Inst. Phys. Conf. Ser.* **142** 609
[34] Bauer A, Kräusslich J, Kocher B, Goetz K, Fissel A and Richter W 1999 *Mater. Sci. Eng.* B **61/62** 179
[35] Northrup J E and Neugebauer J 1995 *Phys. Rev.* B **52** R17001
[36] Powell J, Larkin D and Abel P 1995 *J. Electron. Mater.* **24** 295
[37] Hallin C, Owman F, Martensson P, Ellison A, Konstantinov A, Kordina O and Janzen E 1997 *J. Cryst. Growth* **181** 241
[38] Ramachandran V, Brady M, Smith A, Feenstra R and Greve D 1998 *J. Electron. Mater.* **27** 308
[39] Nakamura S, Kimoto T, Matsunami H, Tanaka S, Teraguchi N and Suzuki A 2000 *Appl. Phys. Lett.* **76** 3412
[40] Xie Z Y, Edgar J H, Burkland B K, George J T and Chaudhuri J 2001 *J. Cryst. Growth* **224** 235
[41] Powell J A *et al* 1991 *Appl. Phys. Lett.* **59** 333
[42] Ohtani N, Katsuno M, Aigo T, Fujimoto T, Tsuge H, Yashiro H and Kanaya M 2000 *J. Cryst. Growth* **210** 613
[43] Cheng C, Needs R J and Heine V 1988 *J. Phys. C: Solid State Phys.* **21** 1049
[44] Käckell P, Furthmüller J and Bechstedt F 1998 *Phys. Rev.* B **58** 1326
[45] Righi M C, Pignedoli C A, Borghi G, Felice R D, Bertoni C M and Catellani A 2002 *Phys. Rev.* B **66** 045320
[46] Kimoto T, Itoh A and Matsunami H 1997 *J. Appl. Phys.* **81** 3494

[47] Heinz K, Starke U, Bernhardt J and Schardt J 2000 *Appl. Surf. Sci.* **162/163** 9
[48] Dillon J A, Schlier R E and Farnsworth H E 1959 *J. Appl. Phys.* **30** 675
[49] van Bommel A J, Crombeen J E and van Tooren A 1975 *Surf. Sci.* **48** 463
[50] Bozso F, Muelhoff L, Trenary M, Choyke W J and Yates J T Jr 1984 *J. Vac. Sci. Technol.* **2** 1271
[51] Adachi S, Mohri M and Yamashina T 1985 *Surf. Sci.* **161** 479
[52] Muehlhoff L, Choyke W J, Bozack M J and Yates J T Jr 1986 *J. Appl. Phys.* **60** 2842
[53] Kaplan R and Parrill T M 1986 *Surf. Sci.* **165** L45
[54] Kaplan R 1989 *Surf. Sci.* **215** 111
[55] Nakanishi S, Tokutaka H, Nishimori K, Kishida S and Ishihara N 1989 *Appl. Surf. Sci.* **41/42** 44
[56] Bermudez V M 1995 *Appl. Surf. Sci.* **84** 45
[57] Nienhaus H, Kampen T U and Mönch W 1995 *Surf. Sci.* **324** L328
[58] Johansson L I, Owman F and Martensson P 1996 *Surf. Sci.* **360** L483
[59] Johansson L I, Owman F, Martensson P, Persson C and Lindefelt U 1996 *Phys. Rev.* B **53** 13803
[60] Johansson L I, Owman F and Martensson P 1996 *Surf. Sci.* **360** 478
[61] Tautz F S, Sloboshanin S, Starke U and Schaefer J A 2000 *Surf. Sci.* **470** L25
[62] Amy F, Enriquez H, Soukiassian P, Storino P F, Chabal Y J, Mayne A J, Dujardin G, Hwu Y K and Brylinski C 2001 *Phys. Rev. Lett.* **86** 4342
[63] Amy F, Soukiassian P, Hwu Y K and Brylinski C 2002 *Phys. Rev.* **65** 165323
[64] Chang C S, Tsong I S T, Wang Y C and Davis R F 1991 *Surf. Sci.* **256** 354
[65] Tsai M H, Chang C S, Dow J D and Tsong I S T 1992 *Phys. Rev.* B **45** 1327
[66] Kulakov M A, Heuell P, Tsvetkov V F and Bullemer B 1994 *Surf. Sci.* **315** 248
[67] Marumoto Y, Tsukamoto T, Hirai M, Kusaka M, Iwami M, Ozawa T, Nagamura T and Nakata T 1995 *Japan. J. Appl. Phys.* **34** 3351
[68] Li L, Tindall C, Takaoka O, Hasegawa Y and Sakurai T 1997 *Surf. Sci.* **385** 60
[69] Simon L, Bischoff J L and Kubler L 1999 *Phys. Rev.* B **60** 11653
[70] King S W, Ronning C, Davis R F and Nemanich R J 1998 *J. Appl. Phys.* **84** 6042
[71] Juillaguet S, Kubler L, Diani M, Bischoff J L, Gewinner G, Wetzel P and Bécourt N 1995 *Surf. Sci.* **339** 363
[72] Diani M, Bischoff J L, Kubler L and Bolmont D 1993 *Appl. Surf. Sci.* **68** 575
[73] Bischoff J L, Dentel D and Kubler L 1998 *Surf. Sci.* **415** 392
[74] Shimomura M, Yeom H, Mun B S, Fadley C, Hara S, Yoshida S and Kono S 1999 *Surf. Sci.* **438** 237
[75] Matko I, Chenevier B, Audier M, Madar R, Diani M, Simon L, Kubler L and Aubel D 2002 *Mater. Sci. Forum* **389–393** 315
[76] Diani M, Simon L, Kubler L, Aubel D, Matko I, Chenevier B, Madar R and Audier M 2002 *J. Cryst. Growth* **235** 95
[77] Schröter B, Winkelmann A and Richter W 2001 *J. Electron. Spectrosc. Relat. Phenom.* **114** 443
[78] Schröter B, Winkelmann A, Fissel A, Lebedev V and Richter W 2001 *Mater. Sci. Forum* **353–356** 227
[79] Winkelmann A, Schröter B and Richter W 2002 *Surf. Sci.* **515** 126
[80] Reimer L 1998 *Scanning Electron Microscopy—Physics of Image Formation and Microanalysis* (Berlin: Springer)
[81] Baba-Kishi K Z 2002 *J. Mater. Sci.* **37** 1715
[82] Michael J R and Eades J A 2000 *Ultramicroscopy* **81** 67
[83] Young K H, James T W, Robinson M, Cardona A H, Suzuki H, Kurosawa H, Yamashita T and Hirai T 1991 *Thin Solid Films* **206** 369
[84] Geier S, Schreck M, Hessmer R, Rauschenbach B, Stritzker B, Kunze K and Adams B L 1994 *Appl. Phys. Lett.* **65** 1781
[85] Mo S, Peiner E, Schlachetzki A, Klockenbrink R and Weber E R 1998 *Mater. Sci. Eng.* B **56** 37
[86] Sweeney F, Trager-Cowan C, Cowan D A, O'Donnell K P, Zubia D, Hersee S D, Foxon C T, Harrison I and Novikov S V 2001 *Phys. Status Solidi* b **228** 533
[87] Trager-Cowan C *et al* 2002 *J. Micr.* **205** 226
[88] Page T F, Mc Hargue C J and White C W 1991 *J. Micr.* **163** 245
[89] Wilkinson A J and Hirsch P B 1997 *Micron* **28** 279
[90] Levchuk B I, Makarov V V, Petrov N N, Trairov Y M and Tsvetkov V F 1987 *Phys. Chem. Mech. Surf.* **4** 2744
[91] Schröter B, Kreuzberg M, Fissel A, Pfennighaus K and Richter W 1998 *Mater. Sci. Forum* **264–268** 355
[92] Wagner G, Doerschel J and Gerlitzke A 2001 *Appl. Surf. Sci.* **184** 55
[93] Reuter K, Schardt J, Bernhardt J, Wedler H, Starke U and Heinz K 1998 *Phys. Rev.* B **58** 10806
[94] Schardt J, Bernhardt J, Starke U and Heinz K 2000 *Phys. Rev.* B **62** 10335
[95] Hollering M *et al* 1998 *Phys. Rev.* B **58** 4992
[96] Seubert A, Bernhardt J, Nerding M, Starke U and Heinz K 2000 *Surf. Sci.* **454–456** 45

[97] Schardt J, Bram C, Müller S, Starke U, Heinz K and Müller K 1995 *Surf. Sci.* **337** 232
[98] Starke U, Schardt J and Franke M 1997 *Appl. Phys.* A **65** 587
[99] Schardt J, Bernhardt J, Franke M, Starke U and Heinz K 1998 *Mater. Sci. Forum* **264–268** 343
[100] Starke U, Bernhardt J, Schardt J and Heinz K 1999 *Surf. Rev. Lett.* **6** 1129
[101] Bernhardt J, Schardt J, Starke U and Heinz K 1999 *Appl. Phys. Lett.* **74** 1084
[102] Sieber N, Mantel B F, Seyller T, Ristein J, Ley L, Heller T, Batchelor D R and Schmeißer D 2001 *Appl. Phys. Lett.* **78** 1216
[103] Sieber N, Stark T, Seyller T, Ley L, Zorman C A and Mehregany M 2002 *Appl. Phys. Lett.* **80** 4726
[104] Starke U 2001 *Mater. Sci. Forum* **353–356** 205
[105] Scharmann F and Pezoldt J 2002 *Mater. Sci. Forum* **389–393** 463
[106] Braun W 1999 *Applied RHEED: Reflection High-Energy Electron Diffraction During Crystal Growth* (Berlin: Springer)
[107] Gajdardziska-Josifovska M and Cowley J M 1991 *Acta Crystallogr.* A **47** 74
[108] Zhukova L A, Evstigneev A M, Prokof'eva N K, Shashkov Y M and Gran Y M 1975 *Kristallografiya* **21** 807
[109] Zhukova L A and Zvyagin B B 1976 *Kristallografiya* **21** 1193
[110] Fadley C S 1992 *Synchrotron Radiation Research: Advances in Surface Science* vol 2, ed R Z Bachrach (New York: Plenum) pp 421–518
[111] Barbieri A and Van Hove M A 1999 private communication (http://electron.lbl.gov/leedpack/)
[112] Tanuma S, Powell C J and Penn D R 1987 *Surf. Sci.* **192** L849
[113] Kono S, Goldberg S M, Hall N F T and Fadley C S 1980 *Phys. Rev.* B **22** 6085
[114] Harris G (ed) 1995 *Properties of Silicon Carbide* (Washington, DC: INSPEC)
[115] Fritzsche V 1989 *Surf. Sci.* **213** 648
[116] Rehr J J, Albers R C, Natoli C R and Stern E A 1986 *Phys. Rev.* B **34** 4350
[117] Chen Y, de Abajo F J G, Chassé A, Ynzunza R X, Kaduwela A P, Van Hove M and Fadley C S 1998 *Phys. Rev.* B **58** 13121
[118] Sambi M and Granozzi G 1999 *Surf. Sci.* **426** 235
[119] Seelmann-Eggebert M and Richter H 1991 *Phys. Rev.* B **43** 9578
[120] Seelmann-Eggebert M 1993 *Phys. Rev.* B **48** 11838
[121] Schieffer P, Jezequel G, Lepine B, Sebilleau D, Feuillet G and Daudin B 2001 *Surf. Sci.* **482–485** 593
[122] Humphreys C J 1979 *Rep. Prog. Phys.* **42** 1825
[123] Spence J C H and Zuo J M 1992 *Electron Microdiffraction* (New York: Plenum)
[124] Bird D M and King Q A 1990 *Acta Crystallogr.* A **46** 202
[125] Doyle P A and Turner P S 1968 *Acta Crystallogr.* A **24** 390
[126] Gao H X and Peng L M 1999 *Acta Crystallogr.* A **55** 926
[127] Hall C and Hirsch P 1965 *Proc. R. Soc.* A **286** 158
[128] Rossouw C J, Miller P R, Josefsson T W and Allen L J 1994 *Phil. Mag.* A **70** 985
[129] Zuo J M, Gjonnes K and Spence J C H 1989 *J. Electron. Microsc. Technol.* **12** 29
[130] Marthinsen K and Høier R 1986 *Acta Crystallogr.* A **42** 484
[131] Dudarev S L, Rez P and Whelan M J 1995 *Phys. Rev.* B **51** 3397
[132] Morniroli J P 2000 *Electron Diffraction* (Lille: Université des Sciences et Technologies)
[133] Winkelmann A, Schröter B and Richter W 2003 *Surf. Sci.* **532–535** 869
[134] Winkelmann A, Schröter B and Richter W 2003 *Ultramicroscopy* **98** 1
[135] Pendry J B 1980 *J. Phys. C: Solid State Phys.* **13** 937
[136] Sabisch M, Krüger P and Pollmann J 1997 *Phys. Rev.* B **55** 10561